COMPUTATIONAL SIMULATION OF PROPELLERS* IN CRUISE

Ethan A. Romander
NASA Ames Research Center
Moffett Field, CA USA

Keywords: *tiltrotor, cruise, propeller, CFD*

Abstract

This paper will present a study of the application of Computational Fluid Dynamics [CFD] to propeller aerodynamic problems. First, in order to show the aptitude of CFD for propeller applications, a CFD solution will be compared to NACA wind tunnel data for a high-speed propeller. Second, the suitability of CFD in proprotor applications will be shown through a comparison to NASA Tilt Rotor Aeroacoustic Model [TRAM] wind tunnel data. Finally, CFD models of the current V-22 proprotor configuration and Sikorsky Aircraft Corporation's Variable Diameter Tilt Rotor [VDTR] configuration will be compared.

1 List of Symbols

A	Propeller disk area
C_P	Power coefficient, $\frac{P}{\rho_\infty A(\Omega R)^3}$
C_T	Thrust coefficient, $\frac{T}{\rho_\infty A(\Omega R)^2}$
n	Propeller shaft speed, RPM
P	Power required to turn propeller
R	Propeller radius
T	Propeller thrust
V_{tip}	Propeller tip speed, ΩR
λ_0	Propeller inflow ratio, $\frac{V_\infty}{V_{tip}}$
Ω	Propeller shaft speed, rad/sec
ρ_∞	Freestream density

*The term propeller will be used to refer to both conventional propellers and to proprotors in cruise. When a distinction between the two is necessary, the terms "proprotor" and "conventional propeller" will be used.

2 Introduction

CFD is rarely used in the design and analysis of propellers. Nevertheless, CFD seems to be a natural choice: propellers employ airfoils at high speeds where the effects of compressibility and three dimensionality are considerable. These effects are best captured by a full, three dimensional Navier-Stokes solution. Unfortunately, Navier-Stokes solutions of most rotating wing devices are traditionally limited by the tendency for non-physical dissipation of vorticity and the substantial computational resource requirements. However, this paper will show that these factors are not as limiting for propeller models.

Computational fluid dynamics is actually ideally suited to propeller applications: The wake generated by the propeller is quickly swept away by the relatively high flight speed. By the time numerical effects have dissipated the wake, it is too far away to significantly influence the solution near the propeller. Furthermore, the isolated propeller problem is steady in a blade fixed reference frame, which greatly simplifies the solution of the Navier-Stokes equations. Finally, there is a periodicity to the propeller problem that is not present in many rotary wing applications. This means that the time to compute a solution can often be reduced proportionally to the number of blades.

Parameter	Helicopter Nomenclature	Conventional Propeller Nomenclature	Conversion
Inflow Ratio	$\lambda_0 = \frac{V_\infty}{V_{tip}}$	$J = \frac{V_\infty}{2nR}$	$J = \lambda_0 \pi$
Thrust Coefficient	$C_T = \frac{T}{\rho_\infty A(\Omega R)^2}$	$C_T = \frac{T}{\rho_\infty n^2 (2R)^4}$	$C_{T,conv.prop.} = \frac{\pi^3}{4} \times C_{T,helicopter}$
Power Coefficient	$C_P = \frac{P}{\rho_\infty A(\Omega R)^3}$	$C_P = \frac{P}{\rho_\infty n^3 (2R)^5}$	$C_{P,conv.prop.} = \frac{\pi^4}{4} \times C_{P,helicopter}$

Table 1 Helicopter and conventional propeller nomenclature.

3 Nomenclature

This paper presents results in terms of typical helicopter nomenclature. A summary of the relationships between helicopter nomenclature and conventional propeller nomenclature is presented in Table 1.

4 Flow Solver

The CFD flow solver used was a version of NASA's Overflow [1]. This Reynolds averaged Navier-Stokes solver has been modified to solve general problems with relative motion between model parts by Meakin [6]. The solver uses Chimera overset grids to model the geometry. Strawn et al. [8] further modified this code to vastly reduce the time required to compute solutions for steady problems and geometries with rotational periodicity.

For the first two CFD simulations in this paper (the NACA propeller and the TRAM), only a single blade was modeled with the remaining blades simulated by periodic boundary conditions. These models were solved using a single Cray T-90 processor. The third and fourth models (the V-22 and VDTR models) took advantage of further work on the Overflow solver. Meakin et al. [7] modified the solver to run efficiently on scalable computers. A consequence of these modifications was that the space between the propeller and the edge of the computational domain can only be populated by Cartesian grids. The periodicity of a three-bladed propeller cannot be represented on a cartesian mesh, so these models were constructed with all blades present. These models were solved in using several SGI Origin 2000 processors.

In all cases, the result of a calculation is a dataset representing fundamental fluid properties at every point in the computational domain. This vast accumulation of data can be mined to discover any number of details about a flow field. The primary interest of this study was to determine the forces acting on the blades of the propeller. This is done in two steps: First, the pressure at the surface of the blade is integrated. Second, skin friction is determined from the velocity profile near the blade surface. The skin friction is integrated and combined with the pressure data to determine the total force applied to the blade. From there it is a simple exercise to determine the basic performance quantities C_T and C_P.

5 Methodology

The goal of this paper will be to illustrate the usefulness of CFD in propeller applications in three steps, each incrementally more difficult than the former. For the first step, the ability of Navier-Stokes solutions to produce reliable quantitative performance measurements will be shown by the simulation of a simple high-speed propeller. The second step is a simulation of the NASA TRAM rotor, intended to show that CFD can produce reliable performance measurements for proprotor geometries as well as conventional propellers. The final step will be to show the usefulness of CFD in the design process by executing a comparison of two competing proprotor de-

signs.

5.1 NACA High-speed Propeller

The NACA propeller was a simple three bladed propeller with a rectangular planform, symmetric NACA 16-series airfoils, and a twist schedule optimized for high-speed flight (see Figure 2). For the original NACA test [2, 3], the propeller was mounted in the middle of a long, 32 inch diameter centerbody. The CFD model for this configuration is shown in Figures 1 and 8. To minimize the computational effort required, only one blade and ⅓ of the shaft is modeled. The remaining portions of the propeller are simulated by periodic boundary conditions. In order to ensure the steadiness of the solution, the centerbody was modeled with an inviscid surface boundary condition.

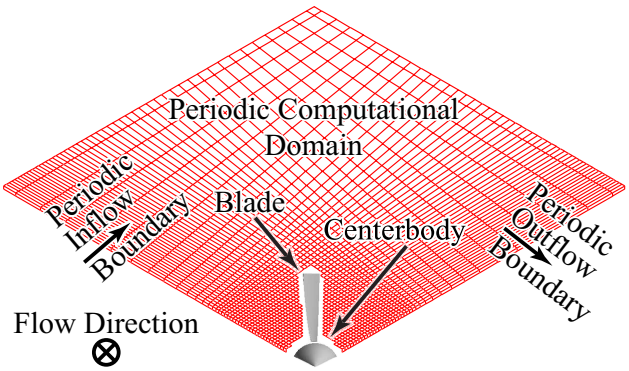

Fig. 1 Model configuration for NACA propeller.

Two cases were considered: one with the propeller operating in a high-transonic speed regime (helical tip Mach number between .75 and .8), and one with the propeller operating in the supersonic speed regime (helical tip Mach number between 1.22 and 1.29). For each case a solution for each of three different inflow ratios (low speed, λ_0 = .267, .362, .417; high speed, λ_0 = .865, .913, .938) was computed. These operating conditions are summarized in greater detail in Table 2. At each inflow ratio, the Navier-Stokes solution was trimmed by adjusting the pitch angle of the blade so that the calculated thrust matched the thrust measured in the wind tunnel. The power required to turn the propeller was then computed and compared with the wind tunnel data.

The CFD model for this propeller consisted of 1.48 million grid points. A single solution required approximately four hours to compute on a single Cray T-90 processor. Three solutions were required in order to trim the propeller to the given thrust coefficient for each operating condition.

5.2 NASA TRAM

The TRAM proprotor [9] is a more complex propeller. The TRAM is approximately a ¼ scale V-22 rotor with its planform, twist distribution, and airfoils designed to be a compromise between its need to serve as both a conventional propeller and a helicopter rotor (see Figure 3). The TRAM rotor was mounted to a nacelle for the wind tunnel test [4]. Recreating this configuration exactly would ruin the steadiness and periodicity possible, therefore the nacelle was omitted in this analysis and an elongated, teardrop-shaped centerbody was substituted. This centerbody mated with the spinner of the rotor and extended two radii in the flow direction (see Figure 4). The centerbody was treated inviscidly in the simulation.

Like the NACA propeller, only one blade of the propeller and ⅓ of the centerbody was actually included in the model. The rest of the geometry was simulated with periodic boundary conditions. The propeller was operated at a helical tip Mach numbers between .63 and .65. Again, solutions for three different inflow ratios (λ_0 = .325, .35, .375) were computed and trimmed to match the thrust measured in the wind tunnel (see Table 3 for details on the operating conditions).

The CFD model for the TRAM propeller consisted of 1.84 million points. A single solution required approximately four hours to compute on a single Cray T-90 processor. Four solutions were required in order to trim the propeller to the required thrust coefficient for each operating condition.

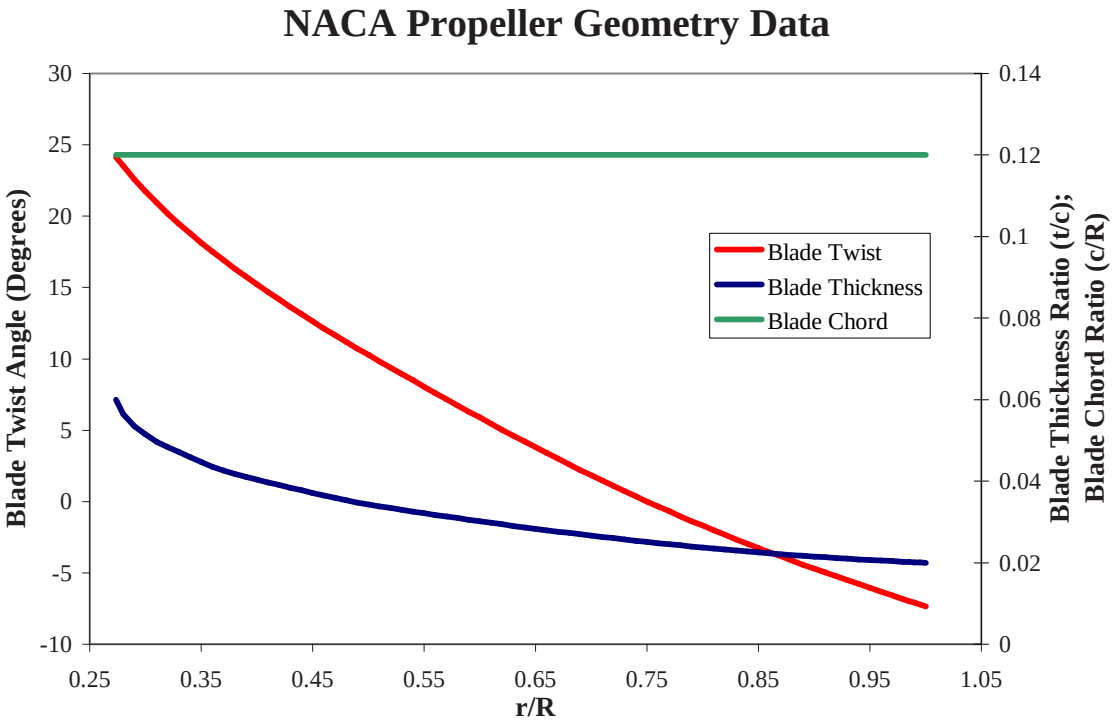

Fig. 2 NACA propeller geometry.

Inflow Ratio	Tip Speed (ft/sec)	Forward Speed (knots)	Helical Mach Number	Thrust Coefficient
.267	817	129	.756	.013125
.362	817	175	.777	0.0
.417	817	201	.791	-.008756
.865	1083	555	1.284	.010829
.913	1027	555	1.246	.004145
.938	999	555	1.228	-.000124

Table 2 Operating conditions for NACA propeller.

Inflow Ratio	Tip Speed (ft/sec)	Forward Speed (knots)	Helical Mach Number	Thrust Coefficient
.325	670.2	129	.631	.002271
.35	670.2	139	.636	.002355
.375	670.2	149	.641	.002571

Table 3 Operating conditions for TRAM propeller.

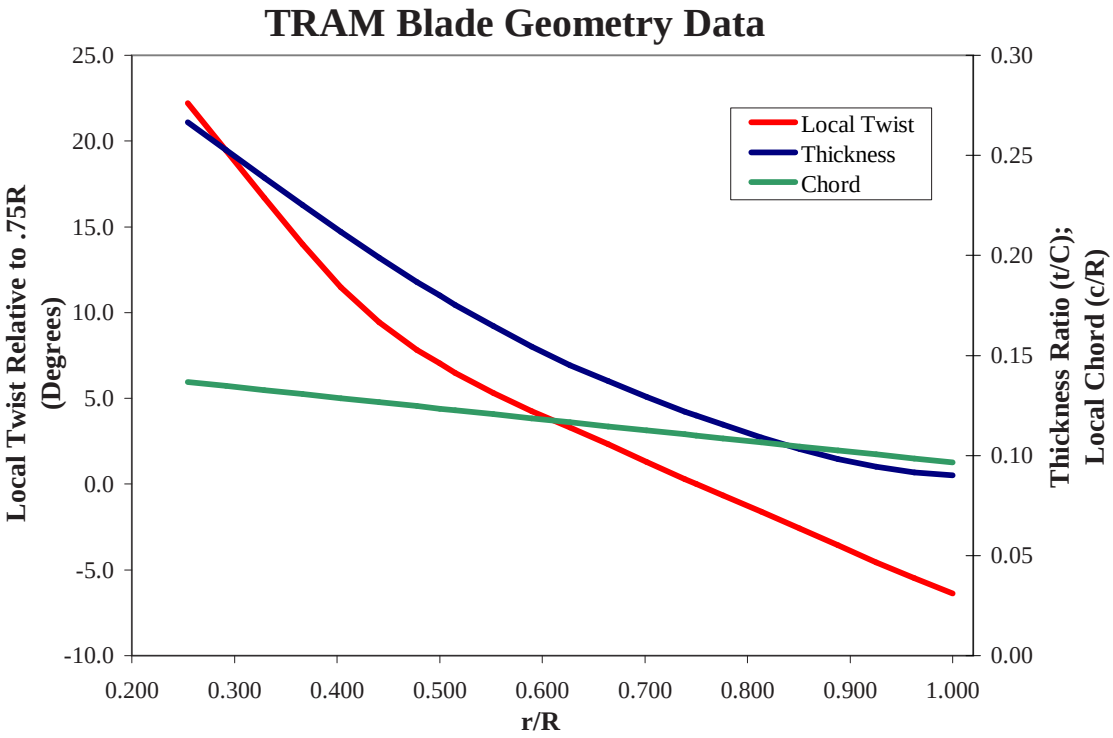

Fig. 3 TRAM propeller geometry.

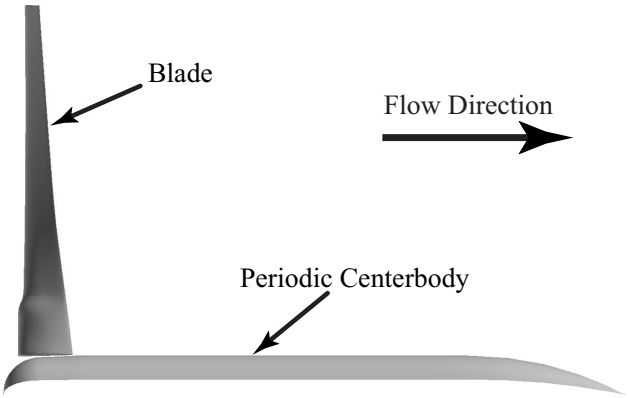

Fig. 4 TRAM model geometry.

5.3 V-22 vs. VDTR

A comparison between the V-22 rotor and the VDTR rotor was arranged in order to demonstrate a practical application of propeller CFD simulation. When in cruise, both of these rotors appear similar: both have three blades, both have the same diameter, and both have similar planforms. However, while the V-22 rotor system suffers from the compromises that must be made between hovering flight and cruise, the VDTR all but eliminates these compromises by enabling the rotor diameter to vary with changing thrust requirements. This allows the twist distribution and planform to be altered for improved cruise performance.

The V-22 rotor is physically similar to the TRAM rotor as presented above except that it is four times larger. The specifics of the VDTR rotor configuration contain information proprietary to Sikorsky Aircraft Corporation and so cannot be reproduced here.

The flight condition was chosen by consider-

ing a typical V-22 cruise condition. This condition involves the V-22 aircraft cruising at 267 kts at 3000 ft on an 84 °F day. According to Kinney et al. [5], the thrust required by the aircraft under this condition is 7761 lb. Thus, each propeller was simulated under these conditions and trimmed to yield 3881 lb of thrust[1].

As mentioned previously, these two models differed from the NACA and TRAM propellers in that they were constructed with all blades present, as opposed to modeling one blade and simulating the other two with periodic boundary conditions. The V-22 model consisted of 10.2 million grid points. Each solution required 21 hours to compute on 48 SGI Origin 2000 processors. A typical CFD representation of the V-22 rotor is shown in Figure 5. The VDTR model required 11 million grid points. Each of these solutions was run on 20 SGI Origin 2000 processors and required 48 hours to compute. Both models required four solutions to trim the propeller to the required thrust coefficient.

6 Results

6.1 NACA High-speed Propeller

Figure 6 summarizes the results of this simulation. The Navier-Stokes model matched the trend of the wind tunnel test very closely, but it under predicted the power required by a nearly constant ΔC_P. Averaged over the three inflow ratios, this ΔC_P is 3.374×10^{-4} for the low speed case and 4.741×10^{-4} for the high speed case.

Inspecting Figure 6, it is clear that the propeller requires substantially more power to operate in the high-speed case than in the low speed case. In addition, the slope of the $C_P - C_T$ curve for the high-speed case is greater than the slope for the low speed case. The reason for this may be obvious to the seasoned aerodynamicist, but inspecting the Navier-Stokes solution reveals the cause to even a novice. Figure 7 shows contours of a shock-finding function for propeller blades operating in both the high-speed and low speed operating conditions. From this image, it is clear that strong shockwaves have formed along the blade in the high-speed case. This indicates that the blade is operating well past the drag divergence mach number and therefore requires correspondingly higher power to operate.

Figure 8 shows a 2-D slice through the flowfield with contours of vorticity magnitude for the NACA propeller. The closed contours indicate the tip vortices from the blades. The tip vortex on the right is from the blade preceding the one shown in the figure. It is clear that the core of this vortex has dissipated by an order of magnitude. The vortex has also been swept downstream nearly two blade radii. This large separation at the time of blade passage means that the dissipation of this tip vortex has little effect on the performance of the rotor. The vortex dissipation would be detrimental to the solution if the inflow ratio were lower—as it would be for a rotor in edgewise flight or a hovering rotor—in which case the blade-vortex passage would occur in closer proximity.

6.2 NASA TRAM

Figure 9 presents the data from the TRAM simulation. Again, the Navier-Stokes solution approached the correct trend, but undershot the wind tunnel data by a nearly constant ΔC_P. Averaging the over the three inflow ratios gives $\Delta C_P = 8.274 \times 10^{-5}$.

6.3 V-22 vs. VDTR

The V-22 propeller and VDTR propeller were simulated as described. To generate the required 3881 lb of thrust at the specified operating condition, the baseline V-22 rotor required 4009 hp. The VDTR rotor was capable of generating the same thrust under the same conditions while requiring only 3607 hp, 10% less than the V-22.

7 Conclusions

Figure 10 illustrates how well the calculated performance data from the NACA propeller and

[1] Since there are two propellers, a single propeller is trimmed to ½ the required thrust

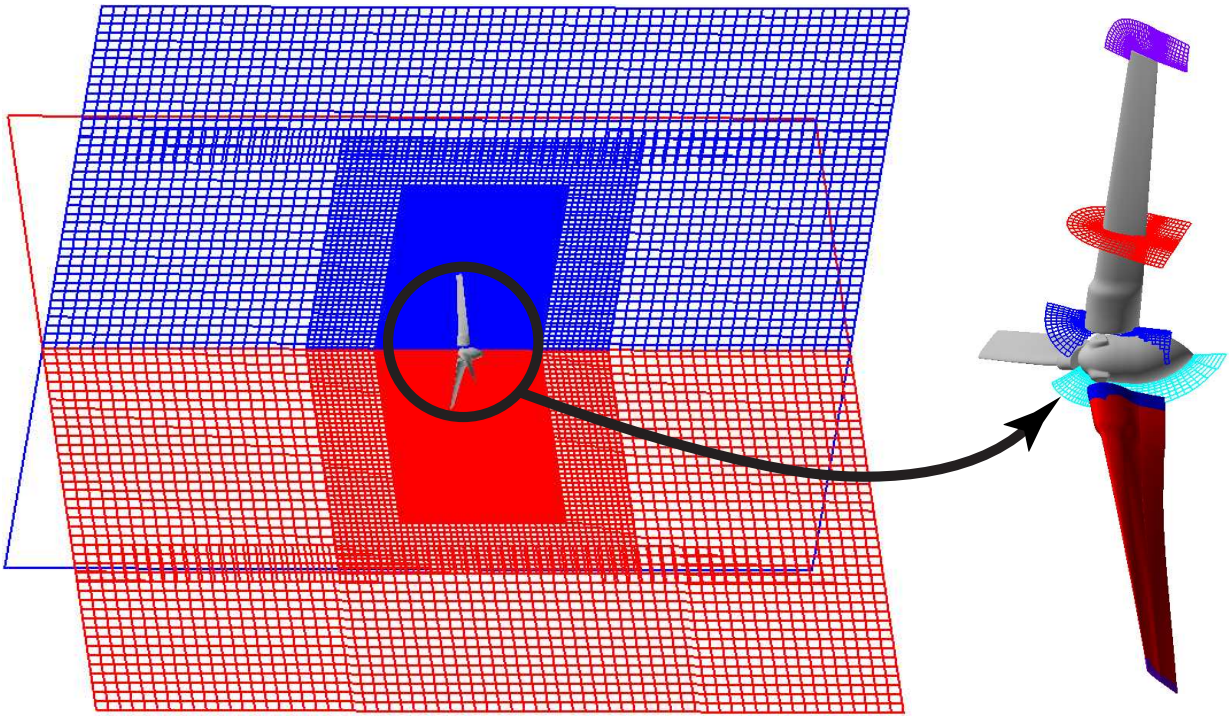

Fig. 5 A typical computational model for the V-22 propeller. The expanse of the computational domain is shown on the left. The blade surface grids are detailed on the right. Flow in this figure moves from left to right.

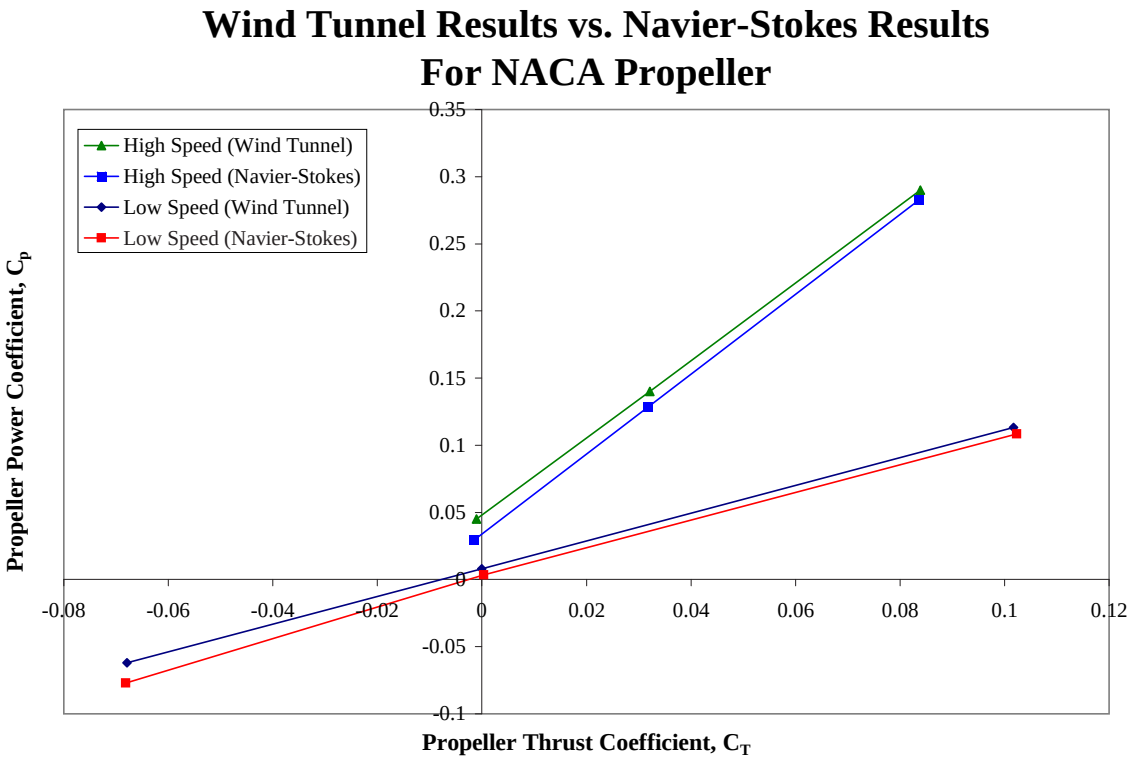

Fig. 6 NACA propeller performance.

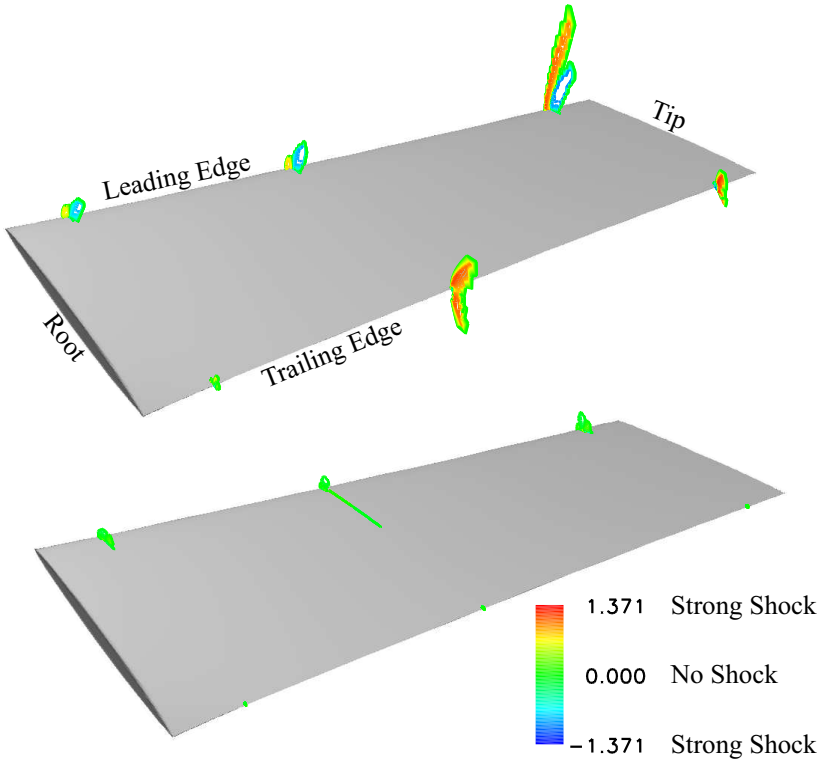

Fig. 7 Contours of shock function for NACA propeller blades operating at $M_{helical} = 1.246$ (top) and $M_{helical} = .756$ (bottom).

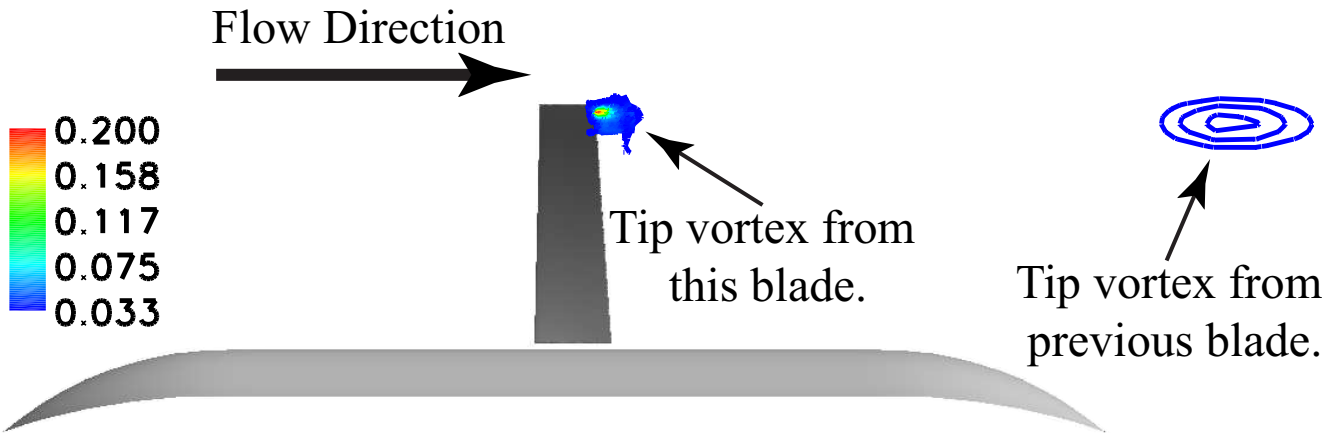

Fig. 8 Vorticity magnitude contours for NACA propeller.

TRAM proprotor models matches the corresponding data measured in wind tunnel tests. Note that all of the points lie above the line of perfect correlation indicating that the Navier-Stokes solution consistently under predicted the power required to operate the rotor at a given condition. The majority of the calculated points fall within 10% of perfect correlation with the wind tunnel experiments. Given that the points remain clustered about the line of perfect correlation under this range of operating conditions, it seems reasonable to expect that Navier-Stokes

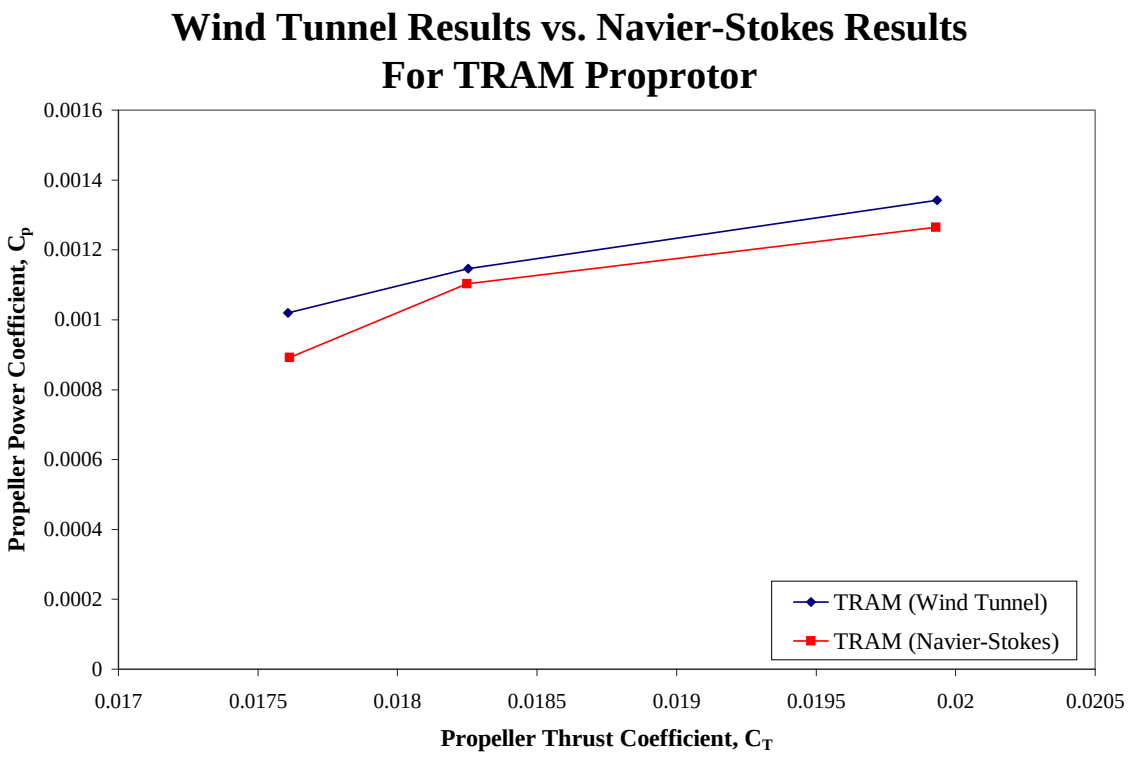

Fig. 9 TRAM propeller performance.

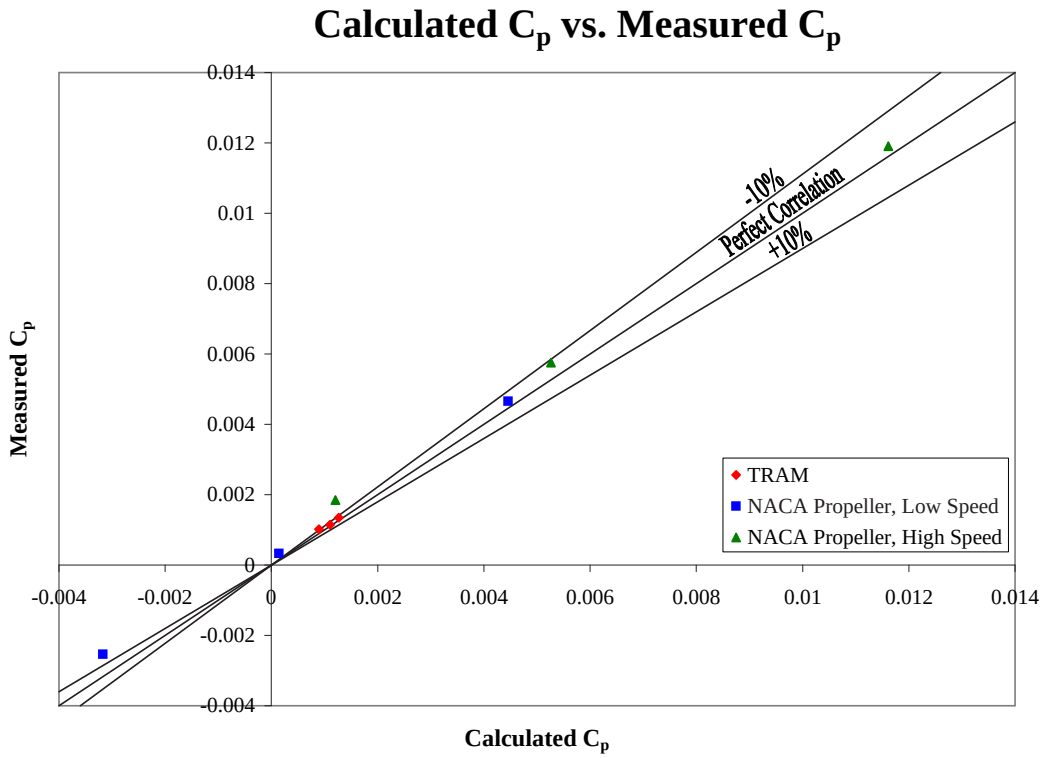

Fig. 10 Solver performance for all NACA propeller and TRAM cases.

calculations will give reasonable estimates of rotor performance (although perhaps slightly under-predicting power) under a wide variety of operating conditions and for a wide variety of propeller types.

This level of accuracy in propeller performance prediction is not unique to Navier-Stokes solution methods. There are many other "conventional" methods currently in use that can equal or exceed the accuracy demonstrated here. Navier-Stokes methods do have a number of advantages, however: Navier-Stokes methods inherently account for compressibility which means that phenomena such as wave drag and shock induced separation are accurately modeled. Navier-Stokes models are fully three dimensional so that effects such as stall delay and shock relief are also accurately represented. Navier-Stokes models are not reliant on airfoil tables which are frequently unavailable for unusual airfoils and operating conditions. Finally, Navier-Stokes solutions are rich in data throughout the flowfield, giving more information about how the propeller interacts with its environment. While other methods may be adjusted to account for some of these differences, they often rely on semi-empirical methods that require case-by-case adjustment or considerable user expertise. Navier-Stokes methods have all of these features built-in.

8 Further Work

An extension of the V-22–VDTR comparison could be constructed to include not just each propeller, but the entire V-22 aircraft. Such a simulation would allow the comparison of the installed performance of each propeller – a more accurate measure of design. This comparison would come at the cost of substantially higher computational resources since the inclusion of the entire fuselage not only adds further geometric complexity but also eliminates the benefits of periodicity and steadiness.

References

[1] Buning P and Jesperson D. e. a. *OVERFLOW User's Manual, Version 1.8g*. NASA Langley Research Center, VA USA, March 1999.

[2] Evans A and Liner G. A wind-tunnel investigation of the aerodynamic characteristics of a full-scale supersonic-type three-blade propeller at mach numbers to 0.96. Report 1375, National Advisory Committee for Aeronautics (NACA), Langley Field, VA USA, May 1953.

[3] Harris F. D. Performance analysis of two early NACA high speed propellers with application to civil tiltrotor configurations. Contractor Report 196702, National Aeronautics and Space Administration, August 1996.

[4] Johnson W. Calculation of tilt rotor aeroacoustic model (TRAM DNW) performance, airloads, and structural loads. *Proc American Helicopter Society Aeromechanics Specialists' Meeting*, Atlanta, GA USA, November 2000.

[5] Kinney D. J and Waters M. H. An evaluation of the V-22 tiltrotor aircraft with variable diameter propeller blades. *Proc AHS International Powered Lift Conference*, Arlington, VA USA, October–November 2000.

[6] Meakin R. On adaptive refinement and overset structured grids. *Proc AIAA 13th Computational Fluid Dynamics Conference*, No AIAA-97-1858, Snowmass, CO USA, June 1997.

[7] Meakin R and Wissink A. Unsteady aerodynamic simulation of static and moving bodies using scalable computers. *Proc AIAA 14th Computational Fluid Dynamics Conference*, No AIAA-99-3302, Norfolk, VA USA, July 1999.

[8] Strawn R and Ahmad J. Computational modeling of hovering rotors and wakes. *Proc AIAA 38th Aerospace Sciences Meeting & Exhibit*, No AIAA-2000-0110, Reno, NV USA, January 2000.

[9] Young L. A. Tilt rotor aeroacoustic model (TRAM): A new rotorcraft research facility. *Proc Heli Japan 98: AHS International Meeting on Advanced Rotorcraft Technology and Disaster Relief*, Nagarafukumitsu, Gifu Japan, April 1998.